SCALE ADAPTATIVE SIMULATION OF THE TURBULENT FLOW INSIDE THE SPIRAL CASING OF A KAPLAN TURBINE

José Gustavo Coelho, josegustavo@unb.br
Luciano Gonçalves Noleto, lucianonoleto@unb.br
Antonio C. P. Brasil Junior, brasiljr@unb.br
Universidade de Brasília, Faculdade de Tecnologia, Departamento de Engenharia Mecânica, Laboratório de Energia e Ambiente, 70910-900 - Asa Norte - Brasília, DF - Brasil

Abstract. *This paper presents results of an unsteady numerical simulation of the turbulent flow inside a spiral casing of a Kaplan Turbine using the SAS SST model. The model used for the flow domain belongs to an empowered Kaplan Turbine installed at Coaracy Nunes plant, located north of the Brazilian amazon. Dynamical loads caused by the flow are causing fatigue failures at the locking pins that hold the hydrofoils. The present work uses the SAS SST turbulence model. This model has a scale adaptative concept, based on the utilization of a Von Kàrman length scale. This characteristic aims to offer LES behavior at unsteady regions of the flow, while offer RANS behavior at steady flow regions. The parallelized version of ANSYS CFX 11 commercial code will be employed to conduct the simulation. Results of streamlines, total pressure contours and torque and pressure signals will be showed. The obtained torque results from that numerical simulation were used to calculate its spectra.*

Keywords: *Spiral casing, Kaplan Turbines, SAS, turbulence.*

1. INTRODUCTION

The flow inside a spiral casing holds great complexity due to the appearance of dynamical stresses over its mechanical parts (Balint et al.(2002), Biswas et al.(2004), Coelho e Brasil Junior (2006), Souza e Brasil Junior (2003)). Those stresses are, in a great part, originated by a complex 3D turbulent flow topology, interacting with turbine structures, in particular with the parts of the spiral casing. Some of its structural stresses are taken into account for the project and design of the casing. Therefore, advanced methodologies of analysis for mechanical and fluid simulation must be employed, since those two problems influence each other. This is an area known as fluid-structure interaction, where knowledge on fluid mechanics, solid mechanics and vibrations are needed. Almost all problems of vibrations in turbomachinery have hydrodynamical origins, such as pressure oscillations and cavitation (Ciocan et al. (2000)). Effects of fluid-structure interactions and the stresses originated by those interactions induce cumulative damage at mechanical parts and fatigue at those parts due to cyclical stresses. Those pathologies force an approximately 10-day halt at the turbine functioning for maintenance.

The analyzed machine is a 25 MW Kaplan Turbine, showed at figure 1. The flow in question involves the water inlet from the dam, until the outlet located at the entrance of the rotor. The hydrodynamic loads at the hydrofoils (guide vanes) are caused mostly by pressure variations over their surfaces. In a full load condition it is expected that the attack angle of the hydrofoils induce a steady, perturbation-free flow, which maximizes the energy production. Drag and Lift forces are directly transmitted to the vanes' axis, and therefore, defining the supported loads at the turbine's mechanical parts. Another load transmitted is the flow torque. The turbulent flow induces time variations at the velocity and pressure fields. Allied with the unpredictability of the turbulence, flow effects at some attack angles can be viewed, such as vortex shedding and boundary layer separation. Those effects compose an unsteady behavior of the flow at the hydrofoil's surroundings, producing variation on the force and torque loads, which can induce cyclical loads at the mechanical parts.

The present paper aims to study the turbulent flow inside the Coaracy Nunes Spiral Casing in a condition of nominal load. Results of a transient numerical simulation conducted by ANSYS CFX commercial code with the SAS SST turbulence model will be presented, as well as torque at the vanes, torque spectra and pressure signals. The following sections will present the Mathematical Formulation of the SAS SST model, the used boundary conditions, qualitative and quantitative results and its conclusions.

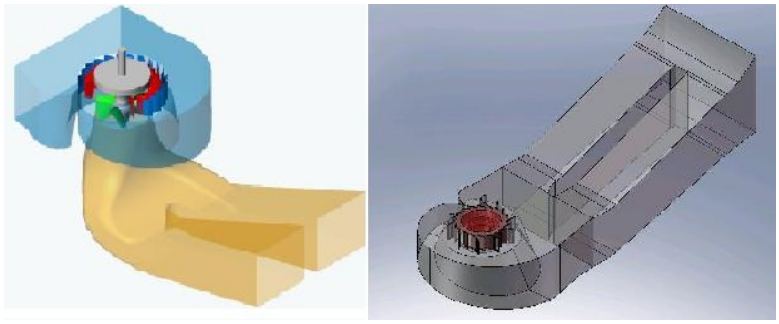

Figure 1. Kaplan turbine

2. MATHEMATICAL FORMULATION

In a framework for turbulence modeling, for incompressible turbulent flows, the conservation of mass, and momentum can be expressed by the classical Reynolds averaged equations given by:

$$\frac{\partial u_i}{\partial x_i} = 0 \tag{1}$$

$$\frac{\partial u_i}{\partial t} + u_j \frac{\partial u_i}{\partial x_j} = -\frac{1}{\rho}\frac{\partial p}{\partial x_i} + \frac{\partial}{\partial x_i}\left[(\nu + \nu_t)\left(\frac{\partial u_i}{\partial x_j} + \frac{\partial u_j}{\partial x_i}\right)\right] \tag{2}$$

In those equations u_i and p are the mean velocity and pressure fields, ν and ν_T are the kinematic and turbulent viscosity, respectively, and ρ is the fluid density.

Menter (Menter et al., 2003) created the SST model, and its principle lies on blending the $k-\varepsilon$ and the $k-\omega$ model. Far from the wall, the model uses the $k-\varepsilon$ formulation, and near the wall, the model uses the $k-\omega$ model. The Scale Adaptative Simulation is a concept based on giving LES behavior in detached flow regions. Using equilibrium assumptions, a standard $k-\varepsilon$ model is transformed into a one equation model, where the Von Kàrman length scale appears at the sink term. This term is responsible to provide dynamical behavior to the model. The model adjusts the resolved scales, developing an energy cascade present in separated turbulent models. The transport equations for the SST model are:

$$\rho\left(\frac{\partial k}{\partial t} + u_i\frac{\partial k}{\partial x_i}\right) = P_k - \beta' k\omega\rho + \frac{\partial}{\partial x_i}\left[\left(\mu + \frac{\mu_t}{\sigma_k}\right)\frac{\partial k}{\partial x_i}\right] \tag{3}$$

$$\rho\left(\frac{\partial \omega}{\partial t} + u_i\frac{\partial \omega}{\partial x_i}\right) = \alpha\rho S^2 + \beta\rho\omega + \frac{\partial}{\partial x_i}\left[\left(\mu + \frac{\mu_t}{\sigma_\omega}\right)\frac{\partial \omega}{\partial x_i}\right] + 2(1-F_1)\rho\sigma_{\omega 2} + \frac{1}{\omega}\frac{\partial k}{\partial x_i}\frac{\partial \omega}{\partial x_i} \tag{4}$$

Here, k and ω are the turbulent kinetic energy and turbulent frequency. The eddy viscosity is defined by:

$$\nu_t = \frac{\alpha_1 k}{\max(\alpha_1\omega, (S_{ij}S_{ij})^{\frac{1}{2}}F_2)} \tag{5}$$

S is an invariant measure of the tensor rate and F_2 is one of two blending functions of the model. The formulation of the blending functions F_1 and F_2 are based on the distance from the surface and on the flow's variables. The blending functions F_1 and F_2 are given as follows:

$$F_1 = \tanh(\arg_1^4) \tag{6}$$

$$\arg_1 = \min\left[\max\left(\frac{\sqrt{k}}{\beta'\omega}, \frac{500\nu}{y^2\omega}\right), \frac{4\rho\sigma_{\omega 2}k}{CD_{k\omega}y^2}\right] \tag{7}$$

$$CD_{k\omega} = \max(2\rho\sigma_{\omega 2}\frac{1}{\omega}\nabla k\nabla\omega, 1, 0.10^{-10}) \tag{8}$$

Here, y is the distance to the wall. F_1 is equal to zero away from the surface ($k-\varepsilon$), and switch over to 1 inside the boundary layer ($k-\omega$ model). F_2 is given by:

$$F_2 = \tanh(\arg_2^2) \tag{9}$$

$$\arg_2 = \max\left(\frac{2\sqrt{k}}{\beta'\omega y}, \frac{500\nu}{y^2\omega}\right) \tag{10}$$

F_2 restrains the limitator for the boundary layer wall. A production limiter is used to avoid the growth of turbulence in stagnation regions:

$$P_k = \mu_t \frac{\partial U_i}{\partial x_j}\left(\frac{\partial U_i}{\partial x_j} + \frac{\partial U_j}{\partial x_i}\right) \tag{11}$$

$$\widetilde{P_k} = \max(P_k, 10 \cdot \rho\beta^* k\omega) \tag{12}$$

The model's constants are accounted by a blend of the corresponding constants of the $k-\varepsilon$ and $k-\omega$ models with the following function:

$$\alpha = \alpha_1 F_1 + \alpha_2(1 - F_1) + ... \tag{13}$$

The constants are $\beta = 0.09$, $\alpha_1 = 5/9$, $\beta_1 = 3/40$, $\alpha_{k1} = 0.5$, $\sigma_{\omega 1} = 0.5$, $\alpha_2 = 0.44$, $\beta_2 = 0.0828$, $\sigma_{k2} = 1$, $\sigma_2 = 0.856$. The analytical expression for ω provided by ω-equation turbulence models allows a near-wall formulation, which gradually switches from wall-functions to low-Re near wall formulations. At the same time, the mesh is refined in wall normal direction.

The ω equation transformed for the SAS model is (Menter and Egorov (2005)):

$$\begin{aligned}\rho\left(\frac{\partial\omega}{\partial t} + u_i\frac{\partial\omega}{\partial x_i}\right) &= \alpha\rho S^2 - \beta\rho(\omega)^2 + \frac{\partial}{\partial x_i}\left[\left(\frac{\mu_t}{\sigma_\omega}\right)\frac{\partial\omega}{\partial x_i}\right] + \frac{2\rho}{\sigma_\Phi}\left(\frac{1}{\omega}\frac{\partial k}{\partial x_i}\frac{\partial\omega}{\partial x_i} - \frac{k}{\omega^2}\frac{\partial\omega}{\partial x_i}\frac{\partial\omega}{\partial x_i}\right) + \\ &+ \zeta_2\kappa\rho S^2\frac{L}{L_{vk}} + \frac{\rho\omega}{k}\frac{\partial}{\partial x_i}\left(\frac{\mu_t}{\rho\sigma_\Phi}\frac{\partial k}{\partial x_i}\right)\left(\frac{1}{\sigma_k} - \frac{1}{\sigma_\Phi}\right) + F_{SAS-SST}\end{aligned} \tag{14}$$

The Von Kàrman length scale is given as follows:

$$L_{vk} = \kappa\left(\frac{\partial u/\partial y}{\partial^2 u/\partial y^2}\right) \tag{15}$$

To preserve the SST model in RANS regime and SAS model in URANS regime, the following condition must be fulfilled:

- For RANS regime:

$$\frac{2\rho}{\sigma_\Phi}\frac{k}{\omega^2}\frac{\partial\omega}{\partial x_i} \approx \zeta_2\kappa\rho S^2\frac{L}{L_{vk}} \tag{16}$$

- For SAS regime:

$$\frac{2\rho}{\sigma_\Phi}\frac{k}{\omega^2}\frac{\partial\omega}{\partial x_i} < \zeta_2\kappa\rho S^2\frac{L}{L_{vk}} \tag{17}$$

L is equal to $\sqrt(k)/C_\mu^{0,25}\omega$, where $C_\mu = 0,09$ and $\kappa = 0,41$. The blending function for the SAS model is given as follows:

$$F_{SAS-SST} = \rho F_{SAS}\max\left[\zeta_2\kappa S^2\frac{L}{L_{vk}} - \frac{2}{\sigma_\Phi}k\max\left(\frac{1}{\omega^2}\frac{\partial\omega}{\partial x_i}\frac{\partial\omega}{\partial x_i}, \frac{1}{k^2}\frac{\partial k}{\partial x_i}\frac{\partial k}{\partial x_i}\right), 0\right] \tag{18}$$

The remaining constants are given as: $F_{SAS} = 1,25$, $\zeta_2 = 1,755$, $\sigma_\Phi = 2/3$. One of the main setbacks of LES is its cost. This methodology demands a fine mesh and sufficient simulation time to resolve all flow scales, which makes LES an expensive alternative for complex geometries. On the other hand, DES' original concept is to restrain LES calculations to separated or detached flow regions, while offer RANS advantages in near wall regions. This trend is justified by the fact that the calculation of a separated region is less expensive than a near-wall calculation in a LES context. But DES is highly dependable of the grid scale. It need to be smaller than the turbulent length scale to provide an accurate calculation of the flow. Besides, for some cases, its computational cost is at the same order than LES. The SAS model is, in fact a URANS model that offer LES behavior on unsteady regions. Its aim is to pose as a feasible and accurate alternative while compared with other transient turbulent modeling, such as LES or DES. The scale L have to be adequate for the flow, for good calculations, which makes this scale the main dependance of the SAS model for accurate simulation (Menter and Egorov (2005)).

2.1 Discretization and Boundary Conditions

The imposed boundary conditions are specified flow rate at the inlet, given by the machine's operation data. The value of the flow rate is set as 143 m^3/s. At the rotor inlet, the case outlet was imposed with a reference pressure condition. No-slip conditions are imposed at the considered walls. The simulation was conducted in a transient fashion on a cluster with the parallelized version of ANSYS CFX commercial code. The imposed simulation timestep is 10^{-3}s. Pressure and torque signals were collected at the surroundings of the blades for analysis. The generated mesh for the case has 6467792 nodes and 21561890 elements. A refinement is made at the vicinity of the vanes, as well as the use of the inflated boundary at them (figures 2 and 2).

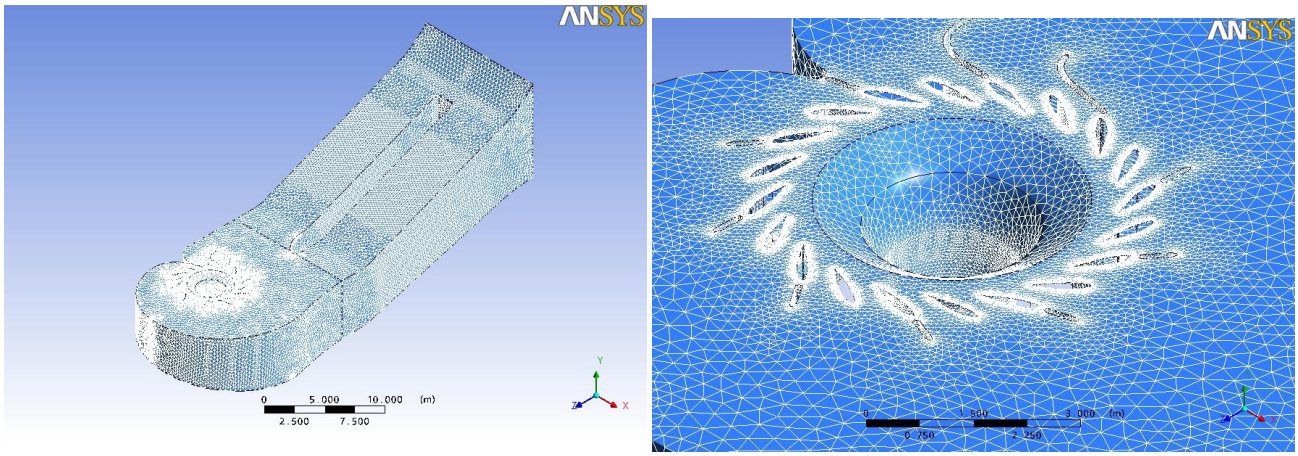

Figure 2. Domain Discretization - Details

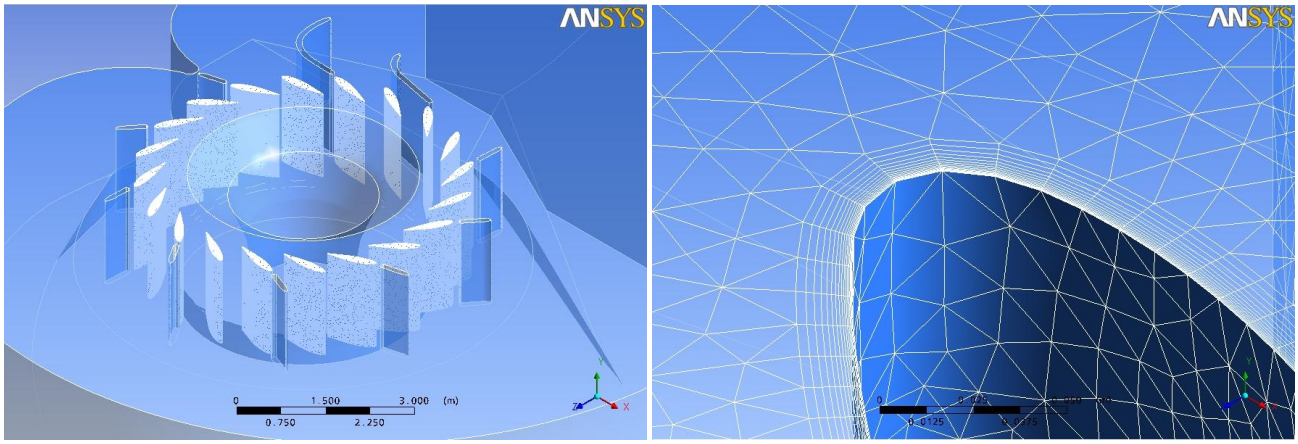

Figure 3. Domain Discretization - Details

3. RESULTS

3.1 Flow Visualizations

Figures 4, 5 and 6 presents the flow patterns at the casing. Its main function is to uniform the flow that goes into the runner. On the great part of the vanes the streamlines and velocity vectors show an adequate flow, where the fixed vanes guide the flow smoothly through the guide vanes. On the other hand, some of the fixed vanes produced some vorticity that affects the flow at the vicinity of the guide vanes. This feature doesn't cause major influence on the global flow, where the flow is perfectly distributed at the runner inlet, which indicates a good vane positioning concerning the attack angle. However, that vorticity makes the local flow unfavorable. It is noted that the recirculation originated by fixed vanes varies with time, which modifies the flow over the guide vane. The velocity field shows a symmetric flow after the vanes and through the runner inlet, which is main goal of the casing. The pressure field shows a decrease at the pressure towards the runner inlet. This field shows the same level of symmetry displayed at the velocity field, which is an expected relationship between velocity and pressure, since when the latter decreases, the first increases.

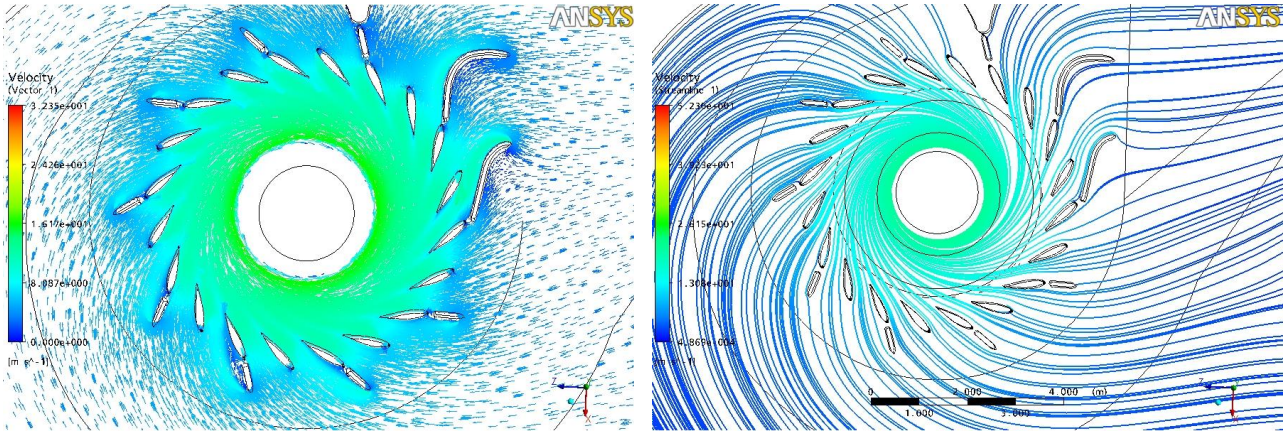

Figure 4. Velocity Vectors and Streamlines

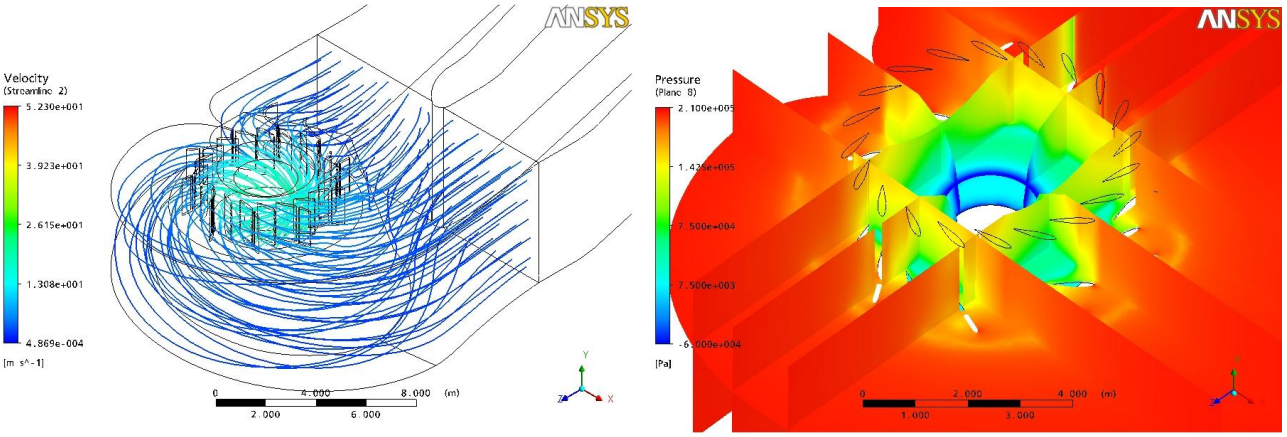

Figure 5. 3D Streamlines and Pressure Contour

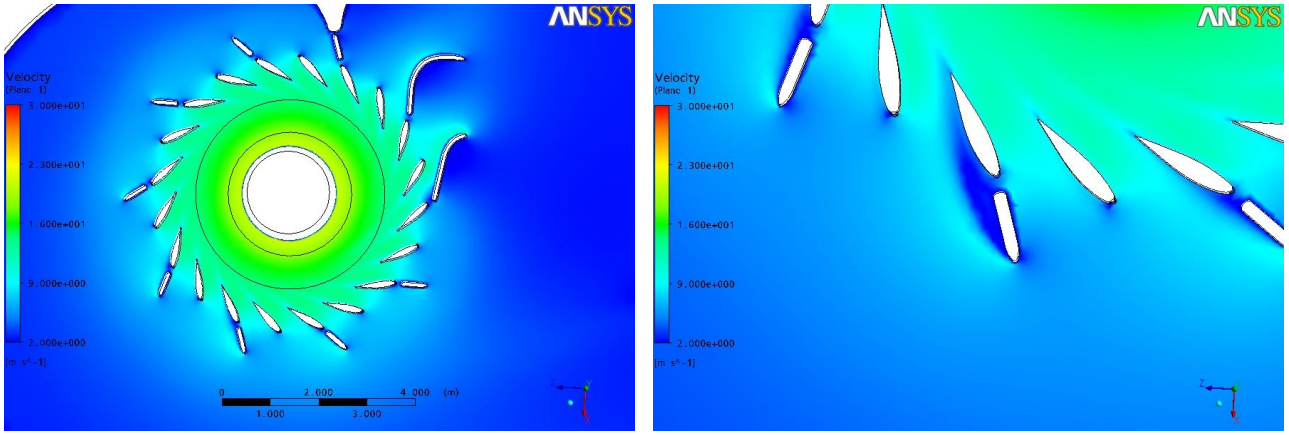

Figure 6. Velocity Contour

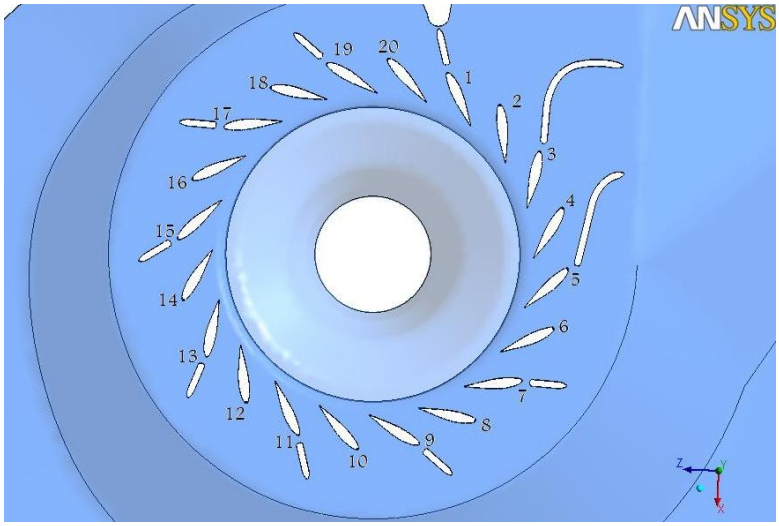

Figure 7. Vane Numbering

3.2 Torque and Pressure Signals

Figure 7 shows the numbering and position of each guide vane, where figures 8 to 10 shows the signals and spectra for the torque at four vanes and figures 11 and 12 shows the pressure signal at the wake of two vanes. Table 1 shows the average torque and its maximum variation. At the torque signals, one can note that the vanes 1 to 8 had shown torque variation below 100 N.m, and the remaining vanes showed variation above this value. Another detail concerns the torque itself. The vanes that presented variation above 100 N.m had presented peaks at its spectra, at a frequency located between 10^{-1} and 10^{-2}. Besides, the larger the variation is, the big the peak comes. This means that, at that frequency, a periodical torque oscillation is occurring. This trend is observed at the torque signal. A periodicity is noted at the signal. As a consequence of that, some vanes are receiving more loads from the flow than others. On the other hand, the vanes that shows variation below 100 N.m presented a more erratic torque signal, and therefore, no pics on the frequency spectrum are observed.The pressure signals showed as well a periodic oscillation, at the order of $1KPa$, which indicates periodical transient behavior from the local flow. The hydrodynamical visualization hasn't shown any vortex shedding, but some vanes had shown variation at its flow topology due to recirculation zones at the stay vanes. This is an indication of transient flow phenomena occurring at the vanes' vicinity. Therefore, a better grid adjustment or an adjustment of the SAS model might be required for better visualization of the flow topology that is causing the periodic oscillation of the torque. On another note, the torque and pressure signals had shown that the flow is inducing a dynamical load at the vanes and, therefore, at its mechanical parts. Those oscillations have the higher value of 654 N.m (Table 1), and there is a vane that presents a negative torque, which indicates an opening load on that vane. Figure 13 shows the torque average tendency values in each vane in a polar format. The negative value in vane 4 is disregarded due to the fact that it indicates an opening tendency induced by the flow on the vane. The observed values, induced in a periodic fashion, can induce mechanical failure and fracture at the mechanical systems.

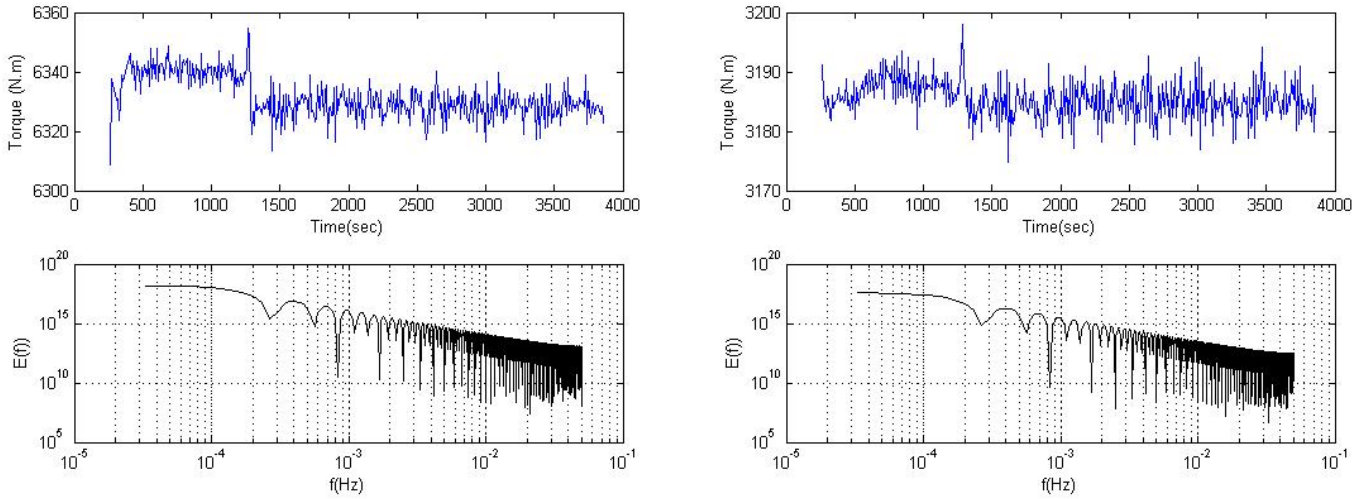

Figure 8. Torque Signal and Spectra at vanes 2 and 5

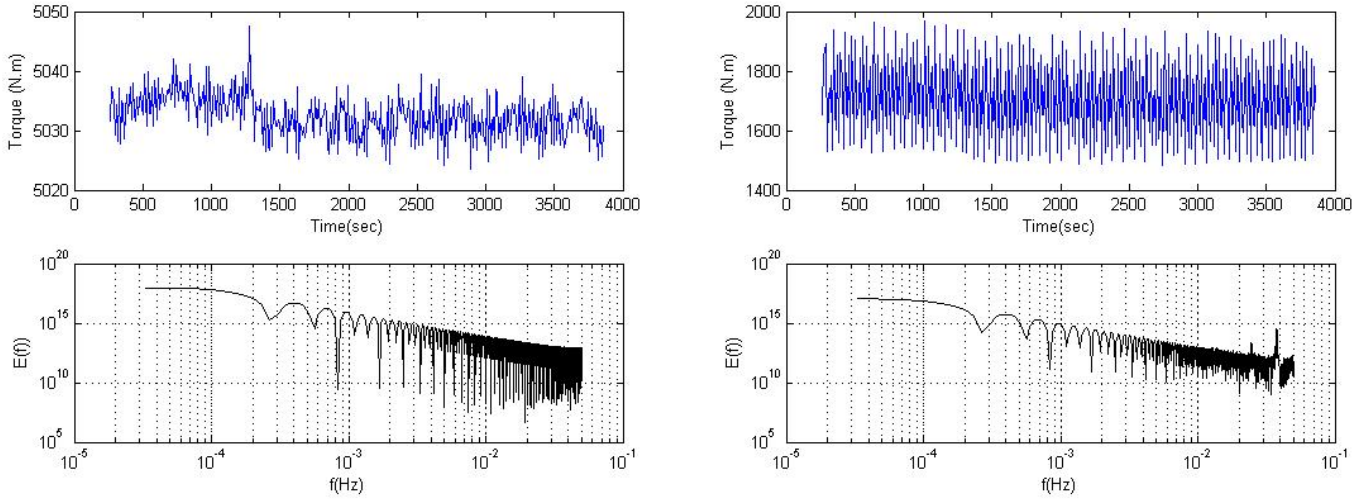

Figure 9. Torque Signal and Spectra at vanes 7 and 11

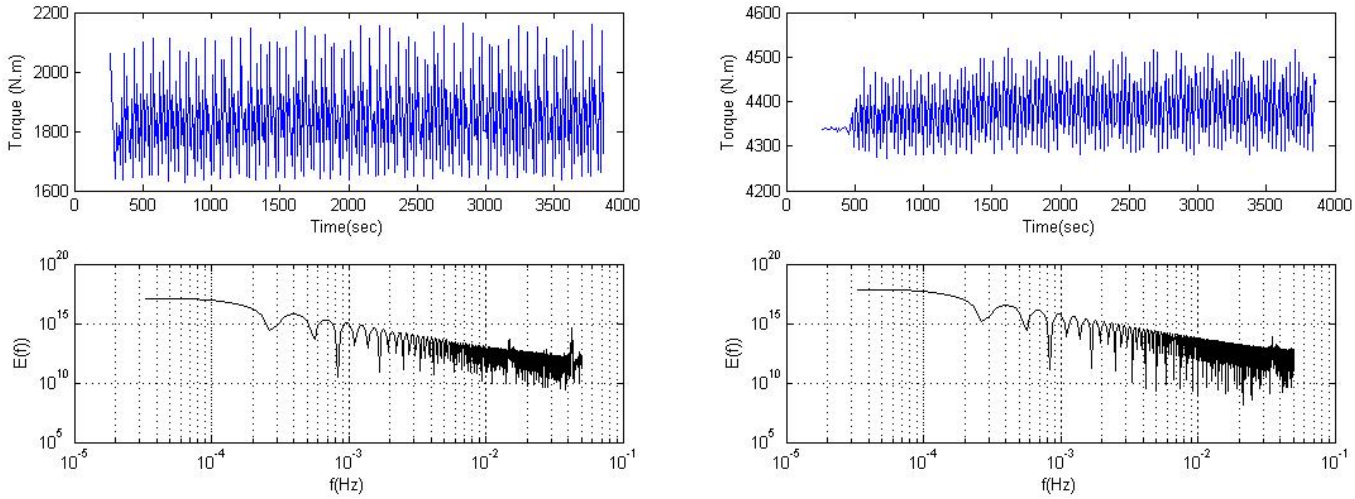

Figure 10. Torque Signal and Spectra at vanes 15 and 17

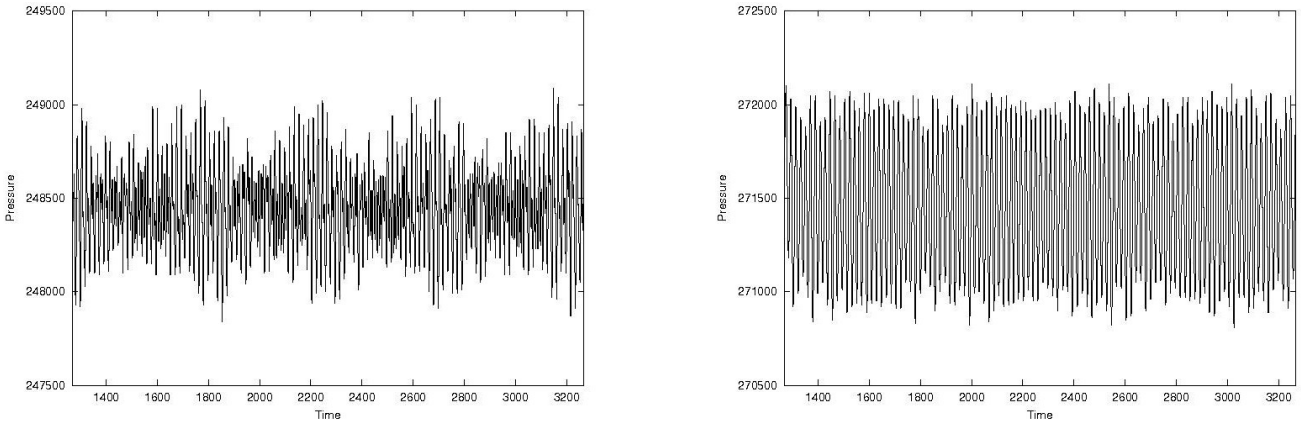

Figure 11. Pressure signals at wakes of vanes 9 and 13 (Pressure at Pa)

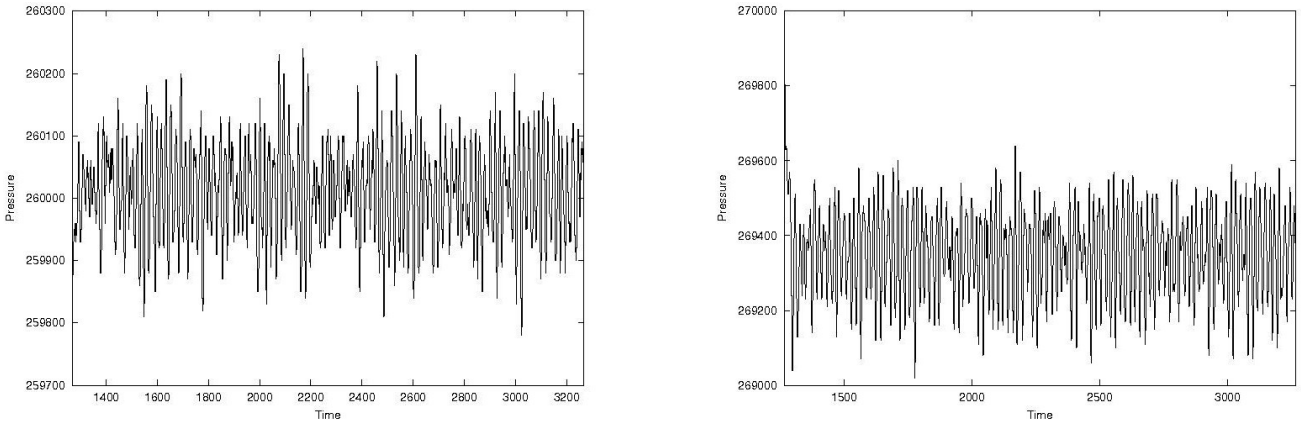

Figure 12. Pressure signals at wakes of vanes 5 and 7 (Pressure at Pa)

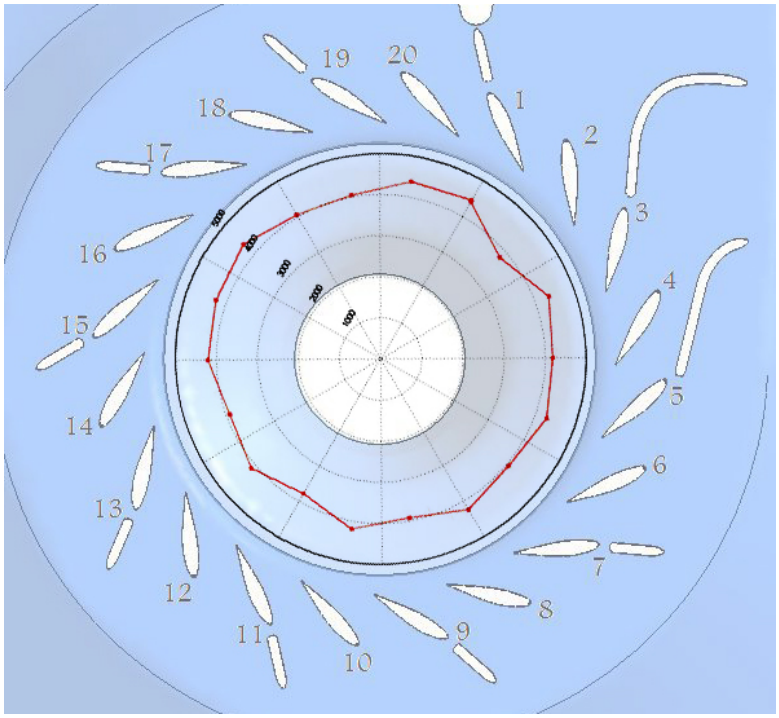

Figure 13. Vane Numbering

Table 1. Average Torque and Maximum Torque Variation (N.m)

Vanes	Average Torque	Maximum Variation
1	7199,7	91,1982
2	6331,6	46,084
3	2957,2	39,4482
4	-8299	67,1846
5	3185,4	23,1895
6	5967,1	37,6729
7	5032,5	24,0425
8	4540,1	79,7622
9	1706,2	486,95
10	3757	267,4214
11	287,08	654,4861
12	4526,7	348,335
13	1846,7	536,4738
14	4974,9	259,0117
15	3133,8	94,4033
16	5330,9	170,1284
17	4381,8	246,9634
18	6139,9	221,3188
19	5271	273,5693
20	6632,6	156,7139

4. CONCLUSIONS

Results of a numerical simulation inside a spiral casing of a Kaplan turbine were presented. Velocity vectors, streamlines, pressure field visualizations, as well as pressure and torque signals, alongside torque spectra were showed.

The effects of the flow direction by the guide vanes were observed, as well as the uniform distribution of the flow. Some of the stay vanes hold an unfavorable flow due to its position. The torque and pressure signals indicate a periodical

variation of the flow. This trend is confirmed by the torque spectra, that showed peaks at a frequency between 10^{-1} and 10^{-2}. This result confirms the oscillatory pattern of the torque, which indicates oscillatory flow phenomena. In order to pinpoint the origin of that phenomenon, further simulations must be conducted.

Therefore, one can conclude that the hydrodynamical characteristics of the flow at the spiral casing ensure project conditions for homogeneous flow at the runner inlet. But the stay vanes generate low-pressure zones that can induce overloads on the guide vanes, noted by the torque and pressure signals

5. REFERENCES

Balint D., Susan-Resiga R., Muntean S., Numerical Simulation of 3D Flow in Kaplan Hydraulic Turbine, Prof. of Classic and Fashion in Fluid Mechanics, Belgrado-Servia, 2002.

Balint D., Susan-Resiga R., Muntean S.,A Numerical Approach for The 3D Flow in Kaplan Turbines, Proc. of Classic and Fashion in Fluid Mechanics, Belgrado-Servia, 2003.

Balint D., Susan-Resiga R., Muntean S., A Numerical Investigation of The Full 3D Turbulent Flow in Kaplan Hydraulic Turbines, 6th International Conference on Hydraulic Machinery and Hydrodynamics Timisoara, Romania, 2004.

Biswas G. Eswaran V., Ghai G., Gupta A., A Numerical Study on Flow Through The Spiral Casing of a Hydraulic Turbine, Int. J. Numer. Meth. Fluids, 28, pp. 143-156, 1998.

Ciocan G.D, Avellan F., Kueny, J.F, Optical measurement techiniques for experimental analysis of hydraulic turbines rotor-stator interaction, Proc. of ASME FEDSM2000, Paper no FEDSM2000-11056, 2000.

Coelho, J.G. ; Brasil Junior, A. C. P. . Estudo numérico de tubos de sucção de turbinas hidráulicas tipo Bulbo. In: 16o Simpósio de Pós-Graduação em Engenharia Mecânica, 2006, Uberlândia. Anais do 16o Posmec. Uberlândia : Universidade Federal de Uberlândia, 2006.

Juillard, J. ; Santos, C. C. B. ; Brasil Junior, A. C. P. . Simulação numérica de turbinas tipo Bulbo. In: 16ž Simpósio de Pós-Graduação em Engenharia Mecânica, 2006, Uberlândia. Anais do 16p Posmec. Uberlândia : Universidade Federal de Uberlândia, 2006.

Menter, F. R., Kuntz, M., and Langtry, R., 2003, "Ten years of industrial experience with the SST turbulence model", Turbulence, heat and Mass transfer, 28.

Menter, F. R., Egorov, Y., 2005, "A Scale-Adaptive Simulation Model using Two-Equation Models", 43rd AIAA Aerospace Sciences Meeting and Exhibit 10-13 January 2005, Reno, Nevada.

Moura, M.D.; Brasil Junior, A. C. P. and Souza, L. C. E. "Assessment of Turbulent Modelling for CFD Simulation In Hydroturbines: Draft Tubes". In: 1st CFX South American Users Conference October, 20-22, 2003 - Florianópolis - SC - Brazil.

Nilsson, H., Andersson, U, and Videhult, S., An experimental investigation of the flow in the spiral casing and distributor of the Holleforsen Kaplan turbine model, Pub. 01-05, Chalmers Univ., Department of Thermo and Fluid Dynamics, 2001.

Souza, L.C.E.O., Brasil Junior, A.C.P., "Assessment of Turbulence Modelling for CFD Simulations Into Hydroturbines: Spiral Casings"p. 1-10, In: 17TH International Congress Of Mechanical Engineering, COBEM 2003, São Paulo: Editora da USP, 2003.

6. Responsibility notice

The author(s) is (are) the only responsible for the printed material included in this paper